

BinaryDemoire: Moiré-Aware Binarization for Image Demoiréing

Zheng Chen ^{*1} Zhi Yang ^{*1} Xiaoyang Liu ¹ Weihang Zhang ² Mengfan Wang ³
 Yifan Fu ² Linghe Kong ¹ Yulun Zhang ^{† 1}

Abstract

Image demoiréing aims to remove structured moiré artifacts in recaptured imagery, where degradations are highly frequency-dependent and vary across scales and directions. While recent deep networks achieve high-quality restoration, their full-precision designs remain costly for deployment. Binarization offers an extreme compression regime by quantizing both activations and weights to 1-bit. Yet, it has been rarely studied for demoiréing and performs poorly when naively applied. In this work, we propose **BinaryDemoire**, a binarized demoiréing framework that explicitly accommodates the frequency structure of moiré degradations. First, we introduce a moiré-aware binary gate (MABG) that extracts lightweight frequency descriptors together with activation statistics. It predicts channel-wise gating coefficients to condition the aggregation of binary convolution responses. Second, we design a shuffle-grouped residual adapter (SGRA) that performs structured sparse shortcut alignment. It further integrates interleaved mixing to promote information exchange across different channel partitions. Extensive experiments on four benchmarks demonstrate that the proposed BinaryDemoire surpasses current binarization methods. Code: <https://github.com/zhengchen1999/BinaryDemoire>.

1. Introduction

Image demoiréing targets the removal of moiré artifacts frequently observed in recaptured images, particularly for screen-captured content. Existing analyses attribute these artifacts to structured aliasing caused by mismatched periodic sampling processes between the display and the camera imaging pipeline. It makes the moiré highly non-stationary and content-dependent (Wang et al., 2023). Such degradations typically appear as directional, multi-scale high-frequency textures, substantially harming perceptual qual-

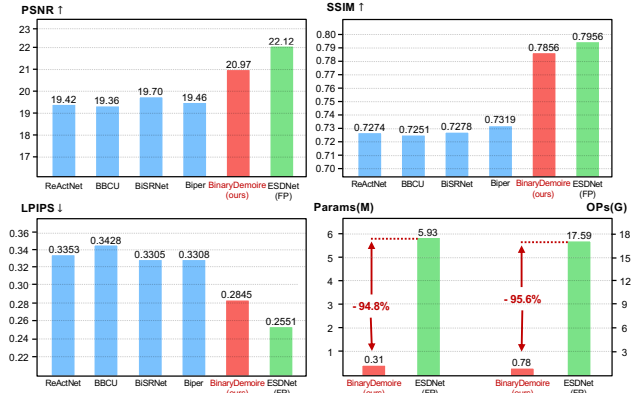


Figure 1. Performance and efficiency comparison between binarization methods and the full-precision baseline model (ESDNet (Yu et al., 2022)). The results are evaluated on the UHDM dataset.

ity. This motivates demoiréing approaches that are both restoration-effective and deployment-efficient.

Recent advancements in deep neural networks have contributed to significant progress in image demoiréing. The demoiréing methods (He et al., 2020; Yu et al., 2022; Zheng et al., 2020) typically build upon multi-scale encoder-decoder backbones (Ronneberger et al., 2015). They enhance cross-scale interaction via stage-wise aggregation (Peng et al., 2024), or explicitly model moiré in the frequency domain through decomposition-based designs (Liu et al., 2025b). Despite favorable restoration performance, these methods often rely on computationally heavy full-precision backbones and dense convolutions. This results in substantial storage and computational overhead. The high complexity makes them less suitable for practical deployment on edge platforms where memory footprint, latency, and energy consumption are tightly constrained.

Model compression and quantization provide a promising direction to bridge the gap between restoration quality and deployability. As an extreme form of quantization, binarization quantizes both activations and weights to 1-bit. It enables the replacement of expensive multiply-accumulate operations with bitwise XNOR-popcount computations, significantly reducing memory and computational cost. Driven by these efficiency benefits, binarization research has gradually expanded from classification to a broader range of low-level vision problems (Xia et al., 2022; Cai et al., 2023; Chen et al., 2024; Vargas et al., 2024; Liu et al., 2025a).

^{*}Equal contribution ¹Shanghai Jiao Tong University ²Tsinghua University ³Virginia Tech. Correspondence to: Yulun Zhang <yulun100@gmail.com>.

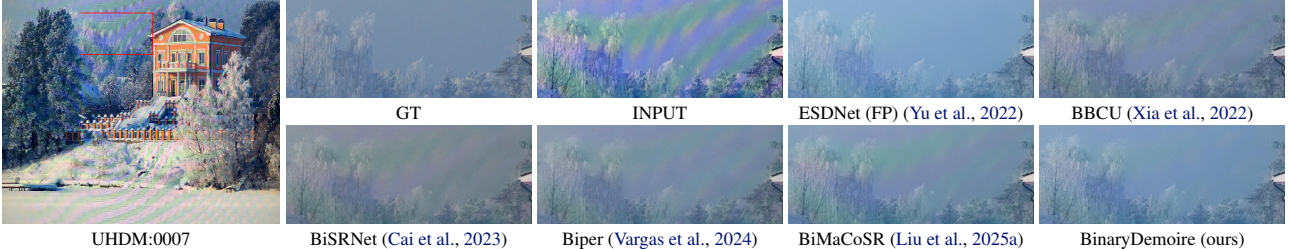


Figure 2. Visual comparison of binarization methods. Our proposed BinaryDemoire outperforms other methods with accurate results.

However, binarizing demoiréing models remains largely under-explored. Applying existing binarization schemes directly to demoiréing backbones often yields suboptimal results. This gap mainly stems from **two** mismatches. **First**, many binarization methods (Rastegari et al., 2016; Liu et al., 2020) adopt distribution-driven parameterization that is largely input-agnostic. However, moiré artifacts are highly structured, frequency-dominated degradations with strong directionality. Thus, uniform binarization incurs pronounced moiré-sensitive quantization errors. **Second**, binary networks (Liu et al., 2018) rely on identity shortcuts to preserve a stable full-precision information path. Yet demoiréing architectures frequently change feature dimension in multi-scale processing, making plain residual connections inapplicable. Although recent methods (Liu et al., 2025a) introduce low-rank full-precision branches to maintain such information flow, their overhead can still be non-negligible. This issue becomes more pronounced when the overall channel width is relatively small, which is common in lightweight restoration backbones.

To address the above challenges, we propose **BinaryDemoire**, an effective binarized demoiréing framework. BinaryDemoire tackles the two mismatches from complementary perspectives. For the **first** issue, we introduce the moiré-aware binary gate (MABG). The module extracts lightweight frequency descriptors together with activation statistics from full-precision features. It then predicts channel-wise gates to condition the aggregation of binary convolution responses. For the **second** issue, we design the shuffle-grouped residual adapter (SGRA) as a lightweight shortcut alignment module. It performs structured sparse 1×1 projection under channel partitioning and integrates an interleaved permutation to promote cross-partition information exchange. As a result, SGRA provides a general and efficient solution for residual alignment under frequent dimensional mismatches, avoiding costly auxiliary branches.

We conduct massive experiments on four demoiréing benchmark datasets. As shown in Figs. 1 and 2, our method significantly outperforms existing binarized approaches. In comparison with the full-precision model (Yu et al., 2022), it achieves comparable performance while reducing more than 90% of the parameters and computational cost. These results demonstrate the advantages of BinaryDemoire.

In general, our contributions can be outlined as follows:

- We propose BinaryDemoire, a binarized framework for image demoiréing. To the best of our knowledge, this is the first work to introduce binarization into demoiréing.
- We design the moiré-aware binary gate (MABG) to adapt to diverse inputs, and the shuffle-grouped residual adapter (SGRA) for easy information propagation.
- Extensive comparisons with existing binarized methods across diverse benchmarks demonstrate the superior performance of BinaryDemoire.

2. Related Work

Image Demoiréing. Image demoiréing aims to remove moiré patterns from captured images. Early demoiréing methods primarily relied on handcrafted priors and traditional signal processing techniques such as smooth filtering (Siddiqui et al., 2009), spectral model (Sidorov & Kokaram, 2002), and sparse matrix decomposition (Liu et al., 2015). These methods typically target specific moiré textures and generalize poorly to diverse real-world patterns. With recent development in deep learning, end-to-end neural methods (Cheng et al., 2019; He et al., 2019; Yu et al., 2022; Xu et al., 2023; Liu et al., 2025b) have been widely adopted for image demoiréing, delivering improved performance. FHDe²Net (He et al., 2020) targets practical high-resolution demoiréing via a cascaded design and frequency-guided content separation. To improve robustness in ultra-high-definition settings, ESDNet (Yu et al., 2022) emphasizes scale robustness and efficiency on 4K data. Meanwhile, Freqformer (Liu et al., 2025b) builds on efficient frequency decomposition to better disentangle high-frequency texture corruption. However, many state-of-the-art demoiréing models remain computationally heavy, making efficient deployment still challenging.

Binarization. Binarization typically compresses the network into 1-bit weights and activations, where parameters are represented as ± 1 , and most multiplications can be replaced by bitwise operations. Binarization research was initially in high-level tasks (Hubara et al., 2016; Rastegari et al., 2016; Liu et al., 2018; 2020; Vargas et al., 2024), which

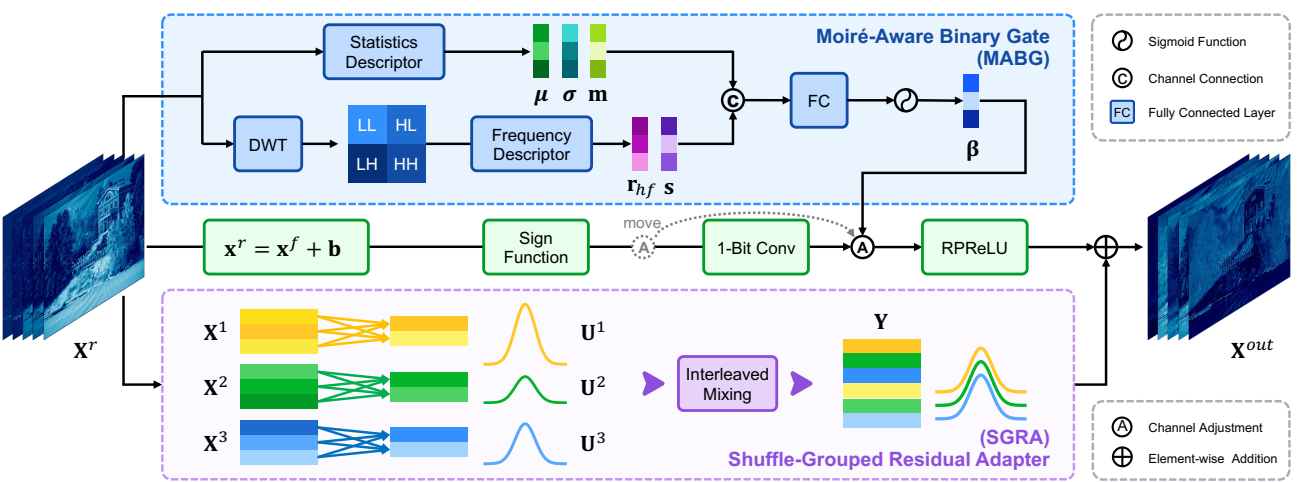


Figure 3. Overview of the BinaryDenoise framework. The BinaryDenoise contains two modules. The first is moiré-aware binary gate (MABG), which adapts binary activation through frequency and statistical descriptors to effectively modulate the binary gate values. The second module is the shuffle-grouped residual adapter (SGRA), which provides lightweight residual alignment across channel and spatial dimensions, enabling effective feature exchange and preserving critical information during the denoising process.

mainly improve the accuracy via improved binary operators and training strategies. Recently, researchers have started to apply binarization to low-level vision tasks (Jiang et al., 2021; Zhang et al., 2024b; Wei et al., 2025). BBCU (Xia et al., 2022) revisits key components in binary convolutions for restoration and proposes a simple binary convolution unit that is effective across typical IR settings. BiSRNet (Cai et al., 2023) further extends binarization to spectral compressive imaging by introducing binarization-aware spectral redistribution. BI-DiffSR (Chen et al., 2024) designs binarization-friendly UNet modules and timestep-aware activation handling. BiMaCoSR (Liu et al., 2025a) combines binarization with one-step distillation and lightweight full-precision auxiliary branches to prevent collapse. Nevertheless, binarized low-level vision models often still suffer from noticeable performance degradation. As far as we are aware, binarization has not yet been systematically investigated for image denoising, motivating us to design a binarized denoising model tailored to moiré artifacts.

3. Methodology

In this section, we introduce our binary denoising framework built on an ESDNet backbone (Yu et al., 2022) for efficient deployment. We first present the overall framework, explaining how we selectively binarize the ESDNet-based pipeline to improve restoration quality and balance computational efficiency. Then, we detail two key designs: the moiré-aware binary gate (MABG), which exploits frequency and statistics descriptors to adaptively modulate binarized activations, and the shuffle-grouped residual adapter (SGRA), which provides lightweight residual alignment under dimensional mismatches.

3.1. Overall Framework

We propose a deployment-friendly binary image denoising framework built upon ESDNet (Yu et al., 2022), a multi-scale encoder-decoder backbone. We focus on binarizing its full-precision convolutions while maintaining restoration fidelity. Specifically, except for the first convolution (which stabilizes the input feature distribution) and the final convolution (which preserves output fidelity), all intermediate convolutional layers are binarized using 1-bit weights and activations. As a result, the main computation is carried out using binarized weights and activations.

Given a full-precision feature tensor $\mathbf{X}^f \in \mathbb{R}^{B \times C \times H \times W}$ and weight $\mathbf{W}^f \in \mathbb{R}^{C_{\text{out}} \times C_{\text{in}} \times K \times K}$, our binarized block (Fig. 3) consists of a binary main branch and a shortcut branch.

Binarization. We first apply a learnable channel-wise threshold $\mathbf{t} \in \mathbb{R}^{1 \times C \times 1 \times 1}$ (Liu et al., 2020) to \mathbf{X}^f and then binarize them with sign function.

$$\mathbf{X}^b = \text{Sign}(\mathbf{X}^f + \mathbf{t}), \mathbf{W}^b = \text{Sign}(\mathbf{W}^f), \quad (1)$$

Let $\mathbf{X}^b \in \{\pm 1\}^{C_{\text{in}} \times H \times W}$ represent the input feature map and $\mathbf{W}^b \in \{\pm 1\}^{C_{\text{out}} \times C_{\text{in}} \times K \times K}$ the binarized convolutional kernels. We introduce an input-channel gate vector $\beta \in \mathbb{R}^{C_{\text{in}}}$ which is predicted from the full-precision input by MABG module and a per-output-channel scaling factor $\alpha \in \mathbb{R}^{C_{\text{out}}}$ ($\alpha = \|\mathbf{W}^f\|_1 / (C_{\text{in}} K^2)$, following the XNOR-Net (Rastegari et al., 2016)). Thus, the channel adjustment convolution output can be written as follows:

$$\mathbf{X}_{\text{out}}^b = (\beta \mathbf{X}^b) * (\alpha \mathbf{W}^b) = \alpha \sum_{c=1}^{C_{\text{in}}} \beta_c (\mathbf{X}_c^b * \mathbf{W}_c^b), \quad (2)$$

where $*$ denotes 2D convolution. The gating coefficients β_c modulate only the channel-wise aggregation of convolution, while the inner products $\mathbf{X}_c^b * \mathbf{W}_c^b$ retain the binary structure. They can be computed via bitwise operations when both activations and weights are 1-bit.

The binary branch performs convolution followed by RPRReLU, and the output is obtained via residual learning:

$$\mathbf{X}^{out} = \text{RPRReLU}(\mathbf{X}_c^b) + \text{SGRA}(\mathbf{X}^f), \quad (3)$$

SGRA(\cdot) is an identity mapping when the shortcut shape matches the main branch, otherwise it applies the proposed shuffle-grouped residual adapter for lightweight projection under channel mismatches (Sec. 3.3).

Training. Since $\text{Sign}(\cdot)$ is not differentiable, we adopt straight-through estimators (STE) (Bengio et al., 2013) for stable end-to-end training. For activation binarization, we use a smooth surrogate $\tanh(\beta x)$ in the backward pass, where β is learnable (Cai et al., 2023).

For weight binarization, we employ a clipped STE to propagate gradients through \mathbf{W}^b , following common practice in binary networks (Courbariaux et al., 2015).

3.2. Moiré-Aware Binary Gate (MABG)

Motivation. Most existing binarization schemes rely on shared, distribution-driven parameterization (Liu et al., 2020; Zhang et al., 2022; Qin et al., 2023b; Zhang et al., 2024a) and largely ignore the frequency structure of task-specific degradations. While this paradigm is often adequate for classification, it is less suitable for image demoiréing. Moiré artifacts typically appear as high-frequency, texture-like patterns with pronounced directionality and substantial variation across scales (He et al., 2020; Campos Zamora et al., 2024). Effective demoiréing, therefore, requires preserving frequency-sensitive information to disentangle moiré components from genuine image details.

Design. Motivated by this mismatch, we propose a wavelet-based moiré-aware binary gate (MABG) that extracts frequency and statistics descriptors and uses them to adjust the binary convolution in a channel-wise manner. The key idea is to explicitly leverage wavelet-derived frequency information to adapt the effective amplitude of binarized activations in a channel-wise manner. Specifically, MABG predicts a gate value $\beta_{b,c}$ from both (i) activation statistics and (ii) wavelet frequency descriptors, and then modulates the binarized convolution by $\beta_{b,c}$. In this way, channels that are more sensitive to moiré frequency patterns can be assigned a more suitable binarization strength, alleviating the severe information loss caused by uniform binarization. We present the detailed procedure of MABG in Algorithm 1. Worth noting is that, to balance computational cost and effectiveness, MABG is applied selectively to key layers, with the specific allocation strategy provided in the supplementary material.

Algorithm 1 Moiré-aware Binary Gate (MABG)

Input: full-precision feature $\mathbf{X}^f \in \mathbb{R}^{B \times C_{in} \times H \times W}$
Output: channel-wise gates $\mathbf{k} \in \mathbb{R}^{B \times C_{in}}$

1) Frequency descriptor

$(\mathbf{X}_{HH}, \mathbf{X}_{HL}, \mathbf{X}_{LH}, \mathbf{X}_{LL}) \leftarrow \text{DWT}(\mathbf{X}^f)$
for $s \in \{HH, HL, LH, LL\}$ **do**

$\mathbf{E}_s \leftarrow \text{MeanAbs}(\mathbf{X}_s)$

end for

$\mathbf{E} \leftarrow \{\mathbf{E}_{HH}, \mathbf{E}_{HL}, \mathbf{E}_{LH}, \mathbf{E}_{LL}\}$

$\mathbf{r}_{hf}, \mathbf{s} \leftarrow \text{Frequency-Descriptor}(\mathbf{E})$

2) Statistics descriptor

$\mu \leftarrow \text{Mean}(\mathbf{X}^f)$

$\sigma \leftarrow \text{Std}(\mathbf{X}^f)$

$\mathbf{m} \leftarrow \text{MeanAbs}(\mathbf{X}^f)$

3) Gate prediction from frequency & statistics

$\mathbf{c} \leftarrow \text{Concat}(\mu, \sigma, \mathbf{m}, \mathbf{r}_{hf}, \mathbf{s})$

$\beta \leftarrow \text{Sigmoid}(\text{FC}(\mathbf{c}))$

return β

Frequency Descriptor. Given a full-precision activation tensor $\mathbf{X} \in \mathbb{R}^{B \times C \times H \times W}$, we use a single-level discrete wavelet transform (DWT) (Yeh et al., 2024; Jiang et al., 2023) to obtain four sub-bands $\{HH, HL, LH, LL\}$, where $\mathbf{X}_i (i \in \{HH, HL, LH, LL\}) \in \mathbb{R}^{C \times h \times w}$ denotes each frequency component, and $h = H/2, w = W/2$.

For each sub-band $s \in \{HH, HL, LH, LL\}$, we compute the mean absolute response as the energy proxy:

$$\mathbf{E}_s = \frac{1}{HW} \sum_{i=1}^H \sum_{j=1}^W |\mathbf{X}_s(i, j)|, \quad (4)$$

Based on these energies, we define two frequency descriptors. The first is the high-frequency ratio \mathbf{r}_{hf} , measuring the proportion of high-frequency energy:

$$\mathbf{r}_{hf} = \frac{\mathbf{E}_{LH} + \mathbf{E}_{HL} + \mathbf{E}_{HH}}{\mathbf{E}_{LL} + \mathbf{E}_{LH} + \mathbf{E}_{HL} + \mathbf{E}_{HH}}, \quad (5)$$

The second descriptor captures the dominant orientation tendency of moiré-like patterns by comparing horizontal with vertical high-frequency bands:

$$\mathbf{s} = \frac{\max(\mathbf{E}_{LH}, \mathbf{E}_{HL})}{\mathbf{E}_{LH} + \mathbf{E}_{HL}}, \quad (6)$$

\mathbf{r}_{hf} reflects how strongly a channel responds to high-frequency structures, while \mathbf{s} indicates whether the response is dominated by a specific orientation.

Statistics Descriptor. Besides frequency descriptor, we also summarize the activation distribution by per-sample, per-channel statistics: mean $\mu_{b,c}$, standard deviation $\sigma_{b,c}$, and mean absolute value $\mathbf{m}_{b,c}$ through a statistics descriptor,

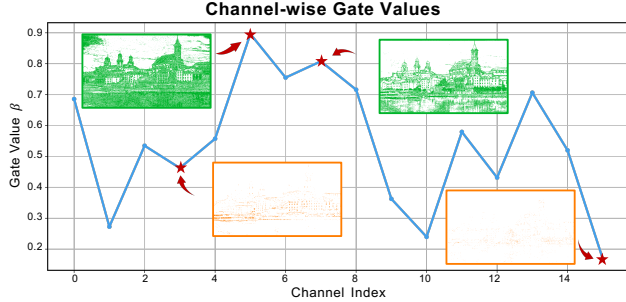


Figure 4. Channel-wise gate values visualization. We visualize the gate values corresponding to different channels, along with their associated binarized feature maps. For channels containing richer high-frequency details, the module learns larger gating responses to increase their contribution. This adaptive strategy highlights informative features and filters out less useful information.

provide valuable insights into the distribution of feature activations, allowing the network to modulate binary activations more effectively (Zhang et al., 2024a).

Gate Prediction From Frequency & Statistics. After concatenating statistics descriptors with the frequency descriptors to form a compact vector, a shared fully connected layer followed by a sigmoid then maps each condition vector to a channel-wise gate (Hu et al., 2018). This design is lightweight due to parameter sharing, yet yields input-adaptive gates for modulating the binary convolution.

$$\beta = \sigma(\text{FC}([\mu, \sigma, m, r_{hf}, s]^\top)). \quad (7)$$

Here, $\text{FC}(\cdot)$ denotes a lightweight shared fully connected layer applied to each per-channel condition vector, and $\sigma(\cdot)$ denotes the sigmoid function.

Figure 4 visualizes the learned channel-wise gate values in our BinaryDemoiré framework. The plot shows how the gate values vary across different channels, where the highlighted regions represent channels with higher or lower gate values. Channels with more prominent features (shown in green) are assigned higher gate values, while those with less significant features (shown in orange) receive lower gate values. This selective modulation helps mitigate the information loss caused by binary activation and improves the network sensitivity to frequency information, particularly in the context of image demoiréing.

3.3. Shuffle-grouped Residual Adapter (SGRA)

Motivation. Residual connections are particularly important for binary networks (Liu et al., 2018; Bethge et al., 2019; Qin et al., 2020), as the identity shortcut provides a stable information path and mitigates the severe representational loss introduced by 1-bit operations. However, in practical demoiréing backbones, channel dimensions and spatial resolutions change frequently due to downsampling, upsampling, or stage-wise feature aggregation. In these cases, a

plain identity shortcut is no longer applicable, and a naive full-precision 1×1 projection introduces non-negligible parameters and computation. Although several methods have been suggested to address this issue, they often deliver suboptimal performance or exhibit limited generalization ability (Chen et al., 2024; Liu et al., 2025a). Therefore, we need a lightweight residual alignment mechanism that preserves the benefits of residual learning under frequent dimensional mismatches.

Design. To address the above issue, we introduce the shuffle-grouped residual adapter (SGRA) as a lightweight shortcut adapter for residual alignment under frequent dimension transitions. SGRA uses a structured sparse channel mapping to substantially reduce parameters and computation, while explicitly maintaining cross-partition information flow through an integrated interleaving scheme. Concretely, our design consists of two complementary components: (i) a partition-wise projection that performs efficient dimension matching within channel subspaces, and (ii) an interleaved mixing strategy that reorganizes channels to promote inter-partition feature exchange before fusion.

Partition-wise Projection. Let $\mathbf{X} \in \mathbb{R}^{B \times C_{\text{in}} \times H \times W}$ be the shortcut input and $\mathbf{U} \in \mathbb{R}^{B \times C_{\text{out}} \times H' \times W'}$ the projected feature before mixing. We set the partition number to the greatest common divisor of the input and output channels, $g = \text{gcd}(C_{\text{in}}, C_{\text{out}})$, so that both C_{in} and C_{out} can be evenly partitioned into g disjoint channel subspaces.

Denote $C_{\text{in}} = g \cdot c_{\text{in}}$ and $C_{\text{out}} = g \cdot c_{\text{out}}$. We perform a structured sparse projection independently within each partition:

$$\mathbf{U}^{(k)}(:, i, j) = \mathbf{W}^{(k)} \mathbf{X}^{(k)}(:, si, sj), \quad (8)$$

$\mathbf{W}^{(k)} \in \mathbb{R}^{c_{\text{out}} \times c_{\text{in}}}$, $k = 1, \dots, g$, where $\mathbf{X}^{(k)}$ and $\mathbf{U}^{(k)}$ denote the k -th channel partition of \mathbf{X} and \mathbf{U} , respectively, and s is the stride used to match spatial resolution when needed. This partition-wise projection serves as a compact residual alignment operator, producing shortcut features that are shape-compatible with the main branch by jointly adjusting channel width and spatial resolution.

Interleaved Mixing. A purely partition-wise projection may lead to isolated representations, which limit information flow across channel subspaces. Inspired by the work (Zhang et al., 2018b), we apply an interleaved channel reordering to the projected feature. Let $m = C_{\text{out}}/g$ and index channels by a partition index $k \in \{0, \dots, g-1\}$ and an intra-partition index $t \in \{0, \dots, m-1\}$. The interleaving is defined as

$$\mathbf{Y}_{:, t \cdot g + k, i, j} = \mathbf{U}_{:, k \cdot m + t, i, j}. \quad (9)$$

which alternates channels from different partitions in the output layout, thereby promoting inter-partition feature exchange before fusion to the binary convolution branch.

Overall, SGRA provides a unified shortcut adaptation paradigm for binarized networks under shape transitions. By combining partition-wise structured projection with interleaved mixing, it produces shape-compatible residual features, retaining full-precision information. It does not rely on costly dense projections or case-specific designs. As a result, SGRA can be seamlessly inserted wherever dimensional mismatches occur, enabling consistent residual learning across the entire multi-scale demoiréing backbone.

4. Experiments

4.1. Experimental Settings

Datasets and Metrics. We perform experiments on four benchmark datasets: UHDM (Yu et al., 2022), FHDMI (He et al., 2020), LCDMoire (Yuan et al., 2019), and TIP2018 (Sun et al., 2018). We evaluate the models using PSNR, SSIM (Wang et al., 2004), and PIPS (Zhang et al., 2018a) metrics for quantitative assessment. For computational cost, the number of parameters(**Params**) is computed as $\text{Params} = \text{Params}^b + \text{Params}^f$, and the number of operations(**OPs**) is computed as $\text{OPs} = \text{OPs}^b + \text{OPs}^f$, where $\text{Params}^b = \text{Params}^f / 32$ and $\text{OPs}^b = \text{OPs}^f / 64$, with the superscripts f and b representing full-precision and binarized modules. This evaluation setup follows previous works on binarized models (Qin et al., 2023a).

Implementation Details. We adopt ESDNet (Yu et al., 2022) as the backbone of our method. All convolution layers, except for the first and last layers, are binarized to 1-bit. The groups number of SGRA is set as $g = \gcd(C_{\text{in}}, C_{\text{out}})$, where C_{in} and C_{out} represent the input and output channel dimensions of the respective convolution layer.

Training Settings. For all four datasets (UHDM, FHDMI, LCDMoiré, and TIP2018), we follow the training procedure of ESDNet (Yu et al., 2022) as closely as possible to ensure reproducibility and fair comparison. In particular, we randomly crop 768×768 patches from training images, set the batch size to 2, and train the models for 150 epochs. We optimize the network using Adam with $(\beta_1, \beta_2) = (0.9, 0.999)$, and set the initial learning rate to 2×10^{-4} , which is scheduled by a cyclic cosine annealing strategy (Loshchilov & Hutter, 2017). All competing methods and our approach are trained under the same data preprocessing and optimization settings on each dataset unless stated otherwise.

4.2. Ablation Study

We perform all ablation experiments on the UHDM dataset. Unless stated otherwise, we follow the identical training procedure as described in Sec. 4.1, and train all variants for 150 epochs. We report the computational complexity in terms of operations (OPs) for a single forward pass, measured on an input of size $3 \times 256 \times 256$.

Break Down. We first examine the effect of each proposed component in Tab. 1a. The baseline is the binarized convolution block from BBCU (Xia et al., 2022) (without MABG and SGRA). Introducing MABG yields a clear improvement in restoration quality, indicating that frequency-conditioned gating reduces critical errors for demoiréing. SGRA further strengthens performance by providing a lightweight, reliable shortcut alignment under frequent dimension transitions. Notably, combining MABG and SGRA achieves the best results, suggesting that modulation in the binarized main branch and structured shortcut adaptation complement.

As shown in Fig. 6, when MABG is applied, the feature maps exhibit a clearer representation of high-frequency components and sharper details, effectively reducing noise. In contrast, without MABG, the feature maps appear more blurred, with a loss of high-frequency information.

Moiré-Aware Binary Gate (MABG). We conduct ablations on MABG in Tab. 1b to verify the effectiveness of its conditioning design. Specifically, we evaluate three simplified variants: (i) conditioning the gate only on frequency descriptors, (ii) conditioning only on activation statistics, and (iii) replacing the conditioned gate with a purely learnable (input-agnostic) gate. The results show that using frequency cues alone or statistics alone consistently underperforms the full design that combines both, indicating that the two sources of information are complementary and jointly important for capturing structured demoiré degradations. Moreover, the purely learnable gate yields inferior performance, suggesting that unguided parameterization is insufficient in this setting. Overall, these comparisons validate that the proposed frequency-and-statistics conditioning is critical for effective gate modulation in binary convolution.

Shuffle-Grouped Residual Adapter (SGRA). We analyze SGRA from three points of view. First, we ablate the proposed interleaved mixing by disabling channel reorganization (w/o Mix) and observe a clear degradation as shown in Tab. 1c, indicating that explicit cross-partition interaction is important for preserving shortcut information beyond independent partition-wise projections.

The visualization in Fig. 5 further illustrates the effect of interleaved mixing by presenting the activation value distributions of the first three channel groups. Before applying Interleaved Mixing, different groups exhibit noticeable distribution shifts and distinct activation patterns, indicating limited interaction and feature sharing across groups. After channel interleaving is introduced, the activation distributions become more aligned and overlapping, suggesting that group discrepancies are effectively reduced.

Second, we compare SGRA with a low-rank shortcut projection where the rank is fixed to 2 to keep the parameter budget comparable. Although both approaches achieve a similar

Table 1. Ablation studies of BinaryDemoire. We report Params (M), OPs (G), and restoration quality (PSNR/SSIM/LPIPS).

(a) Break-down ablation.

Method	Params(M)	Ops(G)	PSNR	SSIM	LPIPS
Base	0.27	0.66	19.36	0.7407	0.3422
+MABG	0.27	0.66	20.18	0.7562	0.3193
+SGRA	0.31	0.78	20.68	0.7820	0.2912
+MABG&SGRA	0.31	0.78	20.97	0.7856	0.2845

(c) Ablation on SGRA.

Method	Params(M)	Ops(G)	PSNR	SSIM	LPIPS
w/o SGRA	0.27	0.66	20.18	0.7562	0.3193
Low-rank ($r=2$)	0.34	0.85	20.87	0.7820	0.2886
w/o Mix	0.31	0.78	20.84	0.7841	0.2884
SGRA	0.31	0.78	20.97	0.7856	0.2845

(b) Ablation on MABG.

Method	Params(M)	Ops(G)	PSNR	SSIM	LPIPS
Freq only	0.31	0.78	20.72	0.7820	0.2896
Stats only	0.31	0.78	20.72	0.7841	0.2904
Learnable	0.32	0.78	20.75	0.7821	0.2990
Freq&Stats	0.31	0.78	20.97	0.7856	0.2845

(d) Ablation of group number.

Method	Params(M)	Ops(G)	PSNR	SSIM	LPIPS
gcd/8	0.59	1.61	21.09	0.7873	0.2899
gcd/4	0.44	1.14	20.98	0.7870	0.2906
gcd/2	0.36	0.90	20.80	0.7867	0.2939
gcd	0.31	0.78	20.97	0.7856	0.2845

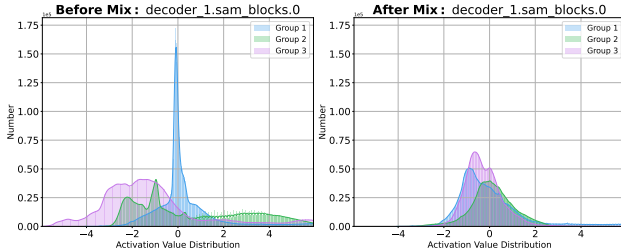


Figure 5. Compare of activation distribution with (w/, right) and without (w/o, left) the interleaved mixing operation. For ease of illustration, we only present the activation distributions of the first three groups.

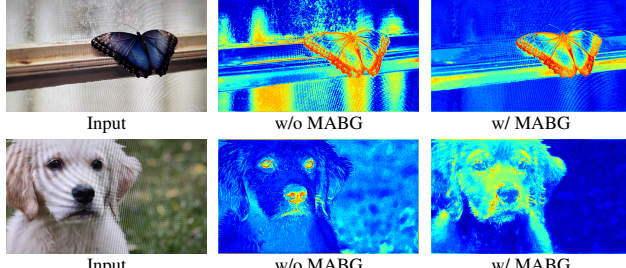


Figure 6. Visualization of feature maps before and after applying MABG. Incorporating MABG enables the module to better focus on the main structure while reducing background interference.

level of compression, the low-rank variant yields inferior performance, as shown in Tab. 1c. This result suggests that SGRA offers a more effective and structurally better-suited mechanism for accommodating frequent channel-width transitions in the binarized backbone.

Finally, we set the partition number to the greatest common divisor of the input and output channels. This choice allows an even split on both sides and leads to stable residual alignment in practice. In contrast, deviating from this setting (e.g., adopting smaller partitions) does not bring consistent improvements and may introduce unnecessary computational overhead, as shown in Tab. 1d.

4.3. Comparison with State-of-the-Art Methods

We evaluate our suggested BinaryDemoire against recent binarization methods, including ReActNet (Liu et al., 2020),

BBCU (Xia et al., 2022), BiSRNet (Cai et al., 2023), Biper (Vargas et al., 2024), and BiMaCoSR (Liu et al., 2025a). All binarization algorithms apply ESDNet (Yu et al., 2022) as the base model. To guarantee a balanced comparison, we match the model size by adjusting the Params of all binarization methods to a similar level.

In addition we compare BinaryDemoire with some of full-precision demoirring models, include MopNet (He et al., 2019), MDDM (Cheng et al., 2019), FHDe²Net (He et al., 2020), and our base model ESDNet (Yu et al., 2022). These comparisons further reflect the performance of our method.

Quantitative Results. We report quantitative comparisons in Tab. 2. We calculate the OPs for a single forward pass with an output image size of $3 \times 256 \times 256$. Compared with the second-best binarized baseline (BiMaCoSR), our BinaryDemoire achieves higher PSNR on both UHDM and TIP2018, with gains of **+0.47 dB** and **+1.29 dB**. Moreover, BinaryDemoire demonstrates competitive performance against existing full-precision methods. For instance, compared with FHDe²Net (He et al., 2020), our method outperforms it on most evaluation metrics on FHDMi.

In terms of efficiency, BinaryDemoire uses 0.31M parameters and 0.78G OPs, which correspond to only **5.2%** of the full-precision base model parameters (a **94.8%** reduction) and **4.4%** of its OPs (a **95.6%** reduction). These impressive results indicate that our BinaryDemoire achieves remarkable performance-efficiency balance under extreme compression, demonstrating its effectiveness and practicality.

Table 2. Comparison with five 1-bit methods and four 32-bit models on four demoiréing benchmarks. ESDNet is the full-precision base model. The highest and second-highest results among binarization methods are colored with red and blue.

Method	Params (M)	Ops (G)	PSNR	UHDM			FHDMi			TIP2018			LCDMoire	
				SSIM	LPIPS	PSNR	SSIM	LPIPS	PSNR	SSIM	PSNR	SSIM	PSNR	SSIM
MopNet (He et al., 2019)	58.57	197.85	19.49	0.7572	0.3857	22.76	0.7958	0.1794	27.75	0.8950	-	-	-	-
MDDM (Cheng et al., 2019)	7.64	30.66	20.09	0.7441	0.3409	20.83	0.7343	0.2515	-	-	42.49	0.9940	-	-
FHDe ² Net (He et al., 2020)	13.57	360.61	20.34	0.7496	0.3519	22.93	0.7885	0.1688	27.78	0.8960	41.40	-	-	-
ESDNet (Yu et al., 2022)	5.93	17.59	22.12	0.7956	0.2551	24.50	0.8351	0.1354	30.11	0.9200	45.34	0.9966	-	-
ReActNet (Liu et al., 2020)	0.31	0.86	19.42	0.7274	0.3353	20.96	0.7629	0.2373	23.96	0.8141	32.75	0.9766	-	-
BBCU (Xia et al., 2022)	0.31	0.86	19.36	0.7251	0.3428	20.34	0.7665	0.2390	24.13	0.8040	32.12	0.9731	-	-
BiSRNet (Cai et al., 2023)	0.33	0.86	19.70	0.7278	0.3305	21.26	0.7737	0.2250	24.47	0.8147	33.83	0.9811	-	-
Biper (Vargas et al., 2024)	0.31	0.86	19.46	0.7319	0.3308	21.05	0.7764	0.2222	23.86	0.8069	32.64	0.9761	-	-
BiMaCoSR (Liu et al., 2025a)	0.31	0.85	20.50	0.7782	0.2896	22.05	0.7943	0.1933	26.04	0.8551	37.70	0.9900	-	-
BinaryDmoire (ours)	0.31	0.78	20.97	0.7856	0.2845	22.47	0.8091	0.1661	27.33	0.8795	39.88	0.9914	-	-

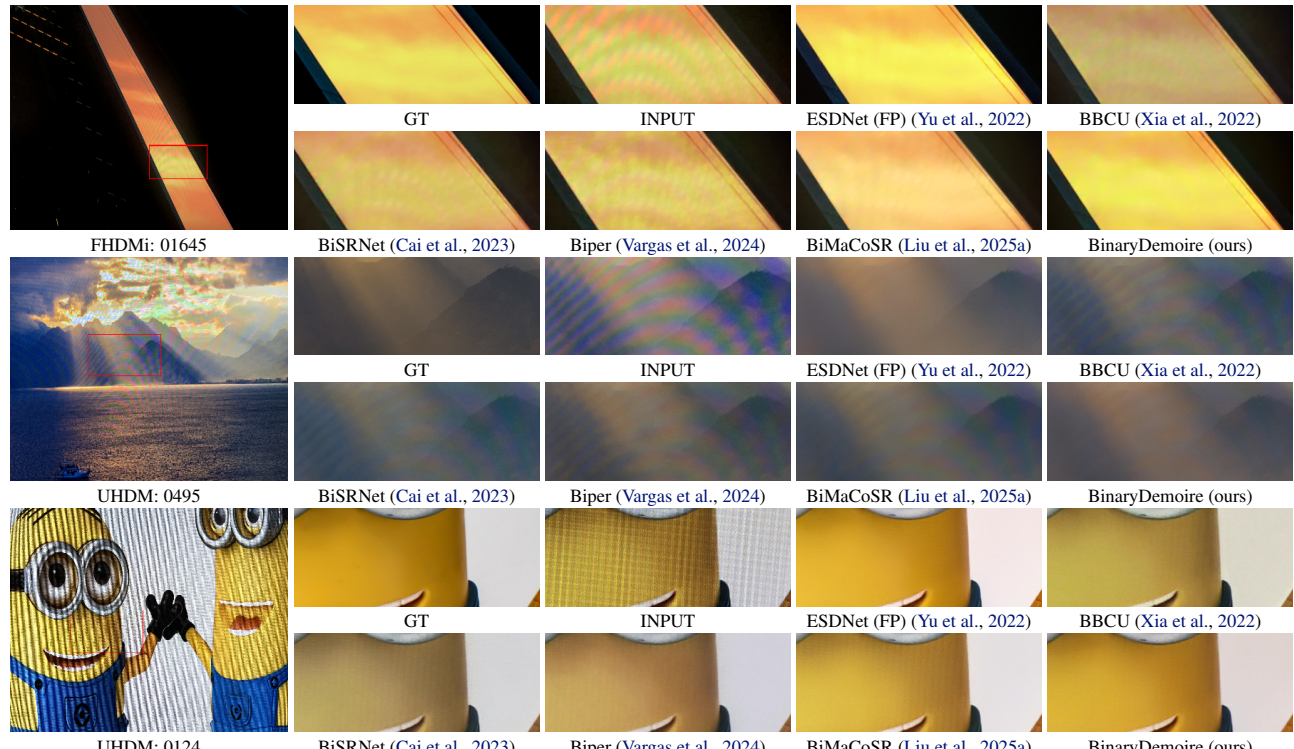


Figure 7. Visual comparison on different datasets, our BinaryDmoire outperforms recent binarization methods

Visual Results. Figure 7 presents visual comparisons of our BinaryDmoire with existing methods across multiple datasets. As shown, our approach is able to restore finer textures and structural details while effectively suppressing complex moiré patterns. In contrast, existing binarized methods tend to introduce artifacts or color distortions. For example, in the first case, compared methods fail to remove severe moiré patterns, whereas our method successfully eliminates the artifacts while preserving accurate color.

Meanwhile, BinaryDmoire achieves outcomes that are much closer to the full-precision version, demonstrating its effectiveness in restoration and computational efficiency. More results are included in the supplementary material.

5. Conclusion

In this paper, we propose the BinaryDmoire, a novel binarized model for image demoiréing. To address the issue of binarization being sensitive to high-frequency noise, we propose the moiré-aware binary gate (MABG). The module adaptively modulates binary convolution responses using lightweight frequency descriptors and activation statistics. We further designed a shuffle-grouped residual adapter (SGRA) to efficiently align residual connections under frequent dimensional mismatches. Extensive experiments on multiple benchmarks demonstrate that BinaryDmoire outperforms existing binarization methods, achieving superior restoration quality with high efficiency.

References

Bengio, Y., Léonard, N., and Courville, A. Estimating or propagating gradients through stochastic neurons for conditional computation. *arXiv preprint arXiv:1308.3432*, 2013.

Bethge, J., Yang, H., Bornstein, M., and Meinel, C. Binaryrydensenet: Developing an architecture for binary neural networks. In *ICCV*, 2019.

Cai, Y., Zheng, Y., Lin, J., Yuan, X., Zhang, Y., and Wang, H. Binarized spectral compressive imaging. In *NeurIPS*, 2023.

Campos Zamora, D., Dogan, M. D., Siu, A. F., Koh, E., and Xiao, C. Moiréwidgets: High-precision, passive tangible interfaces via moiré effect. In *CHI*, 2024.

Chen, Z., Qin, H., Guo, Y., Su, X., Yuan, X., Kong, L., and Zhang, Y. Binarized diffusion model for image super-resolution. In *NeurIPS*, 2024.

Cheng, X., Fu, Z., and Yang, J. Multi-scale dynamic feature encoding network for image demoiréing. In *ICCVW*, 2019.

Courbariaux, M., Bengio, Y., and David, J.-P. Binaryconnect: Training deep neural networks with binary weights during propagations. In *NeurIPS*, 2015.

He, B., Wang, C., Shi, B., and Duan, L.-Y. Mop moire patterns using mopnet. In *ICCV*, 2019.

He, B., Wang, C., Shi, B., and Duan, L.-Y. Fhde2net: Full high definition demoiréing network. In *ECCV*, 2020.

Hu, J., Shen, L., and Sun, G. Squeeze-and-excitation networks. In *CVPR*, 2018.

Hubara, I., Courbariaux, M., Soudry, D., El-Yaniv, R., and Bengio, Y. Binarized neural networks. In *NeurIPS*, 2016.

Jiang, X., Wang, N., Xin, J., Li, K., Yang, X., and Gao, X. Training binary neural network without batch normalization for image super-resolution. In *AAAI*, 2021.

Jiang, X., Wang, N., Xin, J., Li, K., Yang, X., Li, J., Wang, X., and Gao, X. Fabnet: Frequency-aware binarized network for single image super-resolution. *TIP*, 2023.

Liu, F., Yang, J., and Yue, H. Moiré pattern removal from texture images via low-rank and sparse matrix decomposition. In *VCIP*, 2015.

Liu, K., Yang, K., Chen, Z., Li, Z., Guo, Y., Li, W., Kong, L., and Zhang, Y. Bimacosr: Binary one-step diffusion model leveraging flexible matrix compression for real super-resolution. *arXiv preprint arXiv:2502.00333*, 2025a.

Liu, X., Qiu, B., Cao, J., Chen, Z., Zhang, Y., and Yang, X. Freqformer: Image-demoiréing transformer via efficient frequency decomposition. *arXiv preprint arXiv:2505.19120*, 2025b.

Liu, Z., Wu, B., Luo, W., Yang, X., Liu, W., and Cheng, K.-T. Bi-real net: Enhancing the performance of 1-bit cnns with improved representational capability and advanced training algorithm. In *ECCV*, 2018.

Liu, Z., Shen, Z., Savvides, M., and Cheng, K.-T. Reactnet: Towards precise binary neural network with generalized activation functions. In *ECCV*, 2020.

Loshchilov, I. and Hutter, F. Sgdr: Stochastic gradient descent with warm restarts. In *ICLR*, 2017.

Peng, Y.-T., Hou, C.-H., Lee, Y.-C., Yoon, A. J., Chen, Z., Lin, Y.-T., and Lien, W.-C. Image demoiréing via multiscale fusion networks with moiré data augmentation. *IEEE Sensors Journal*, 2024.

Qin, H., Gong, R., Liu, X., Bai, X., Song, J., and Sebe, N. Binary neural networks: A survey. *PR*, 2020.

Qin, H., Zhang, M., Ding, Y., Li, A., Cai, Z., Liu, Z., Yu, F., and Liu, X. Bibench: Benchmarking and analyzing network binarization. In *ICML*, 2023a.

Qin, H., Zhang, X., Gong, R., Ding, Y., Xu, Y., and Liu, X. Distribution-sensitive information retention for accurate binary neural network. *IJCV*, 2023b.

Rastegari, M., Ordonez, V., Redmon, J., and Farhadi, A. Xnor-net: Imagenet classification using binary convolutional neural networks. In *ECCV*, 2016.

Ronneberger, O., Fischer, P., and Brox, T. U-net: Convolutional networks for biomedical image segmentation. In *MICCAI*, 2015.

Siddiqui, H., Boutin, M., and Bouman, C. A. Hardware-friendly descreening. *TIP*, 2009.

Sidorov, D. N. and Kokaram, A. C. Suppression of moiré patterns via spectral analysis. In *VCIP*, 2002.

Sun, Y., Yu, Y., and Wang, W. Moiré photo restoration using multiresolution convolutional neural networks. *TIP*, 2018.

Vargas, E., Correa, C. V., Hinojosa, C., and Arguello, H. Biper: Binary neural networks using a periodic function. In *CVPR*, 2024.

Wang, C., He, B., Wu, S., Wan, R., Shi, B., and Duan, L.-Y. Coarse-to-fine disentangling demoiréing framework for recaptured screen images. *TPAMI*, 2023.

Wang, Z., Bovik, A. C., Sheikh, H. R., and Simoncelli, E. P. Image quality assessment: from error visibility to structural similarity. *TIP*, 2004.

Wei, R., Liu, Z., Fan, Y., Wang, R., Huang, R., and Li, M. Scales: Boost binary neural network for image super-resolution with efficient scalings. In *2025 Design, Automation & Test in Europe Conference (DATE)*, 2025.

Xia, B., Zhang, Y., Wang, Y., Tian, Y., Yang, W., Timofte, R., and Van Gool, L. Basic binary convolution unit for binarized image restoration network. In *ICLR*, 2022.

Xu, S., Song, B., Chen, X., and Zhou, J. Image demoiréing in raw and srgb domains. *arXiv preprint arXiv:2312.09063*, 2023.

Yeh, C.-H., Lo, C., and He, C.-H. Multibranch wavelet-based network for image demoiréing. *Sensors*, 2024.

Yu, X., Dai, P., Li, W., Ma, L., Shen, J., Li, J., and Qi, X. Towards efficient and scale-robust ultra-high-definition image demoiréing. In *ECCV*, 2022.

Yuan, S., Timofte, R., Slabaugh, G., Leonardis, A., Zheng, B., Ye, X., Tian, X., Chen, Y., Cheng, X., Fu, Z., et al. Aim 2019 challenge on image demoiréing: Methods and results. In *ICCVW*, 2019.

Zhang, G., Zhang, Y., Yuan, X., and Fu, Y. Binarized low-light raw video enhancement. In *CVPR*, 2024a.

Zhang, J., Su, Z., Feng, Y., Lu, X., Pietikäinen, M., and Liu, L. Dynamic binary neural network by learning channel-wise thresholds. In *ICASSP*, 2022.

Zhang, R., Isola, P., Efros, A. A., Shechtman, E., and Wang, O. The unreasonable effectiveness of deep features as a perceptual metric. In *CVPR*, 2018a.

Zhang, X., Zhou, X., Lin, M., and Sun, J. Shufflenet: An extremely efficient convolutional neural network for mobile devices. In *CVPR*, 2018b.

Zhang, Y., Qin, H., Zhao, Z., Liu, X., Danelljan, M., and Yu, F. Flexible residual binarization for image super-resolution. In *ICML*, 2024b.

Zheng, B., Yuan, S., Slabaugh, G., and Leonardis, A. Image demoiréing with learnable bandpass filters. In *CVPR*, 2020.